Bioconjugate Chemistry

pubs.acs.org/bc

Article

# Biotin–NeutrAvidin Mediated Immobilization of Polymer Micro- and Nanoparticles on T Lymphocytes

Maxime Ayer, Olivier Burri, Romain Guiet, Arne Seitz, Elisa Kaba, Britta Engelhardt,* and Harm-Anton Klok*

Cite This: *Bioconjugate Chem.* 2021, 32, 541–552

Read Online

ACCESS | Metrics & More | Article Recommendations | Supporting Information

**ABSTRACT:** Cells are powerful carriers that can help to improve the delivery of nanomedicines. One approach to use cells as carriers is to immobilize the nanoparticulate cargo on the cell surface. While a plethora of chemical conjugation strategies are available to bind nanoparticles to cell surfaces, only relatively little is known about the effects of particle size and cell type on the surface immobilization of nanoparticles. This study investigates the biotin–NeutrAvidin mediated immobilization of model polymer nanoparticles with sizes ranging from 40 nm to 1 $\mu$m on two different T cell lines, viz., human Jurkat cells as well as mouse SJL/PLP7 T cells, which are of potential interest for drug delivery across the blood–brain barrier. The nanoparticle cell surface immobilization and the particle surface concentration and distribution were analyzed by flow cytometry and confocal microscopy. The functional properties of nanoparticle-modified SJL/PLP7 T cells were assessed in an ICAM-1 binding assay as well as in a two-chamber setup in which the migration of the particle-modified T cells across an in vitro model of the blood–brain barrier was studied. The results of these experiments highlight the effects of particle size and cell line on the surface immobilization of nanoparticles on living cells.

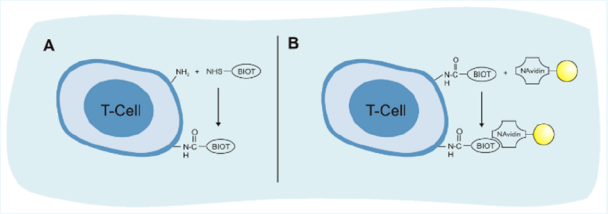


## INTRODUCTION

Circulatory cells have received increasing attention as carriers for the delivery of synthetic nano- and microparticle-based therapeutics.[1−15] Cell-based delivery systems hold enormous promise to help overcome some of the limitations of nano- and microparticle therapeutics. This includes, among others, the possibility to allow highly specific targeted delivery,[16] to facilitate transport across challenging physiological barriers, as well as the opportunity to generate long circulating delivery systems.[17]

One way to use circulatory cells as carriers for therapeutic nano- and microparticles involves the immobilization of the particle-based cargo on the cell surface.[18] A broad variety of chemical approaches, which include both covalent and noncovalent strategies, has been used to immobilize particles on the surface of living cells. Covalent immobilization of particles on living cells has been accomplished by coupling active ester-modified nanoparticles to amino groups present on the cell surface, by reaction between maleimide-functional nanoparticles and thiol groups on the cell surface or via bioorthogonal click reactions between alkyne functionalized nanoparticles and azide groups, which can be introduced to the cell surface via metabolic engineering strategies.[19−23] Alternatively, nano- and microsized particle cargo has been immobilized on the surface of cells by exploiting electrostatic interactions, by lipid insertion in the cell membrane, via binding of wheat-germ agglutinin (WGA) modified particles to *N*-acetylglucosamine and sialic acid resides that are present in the cell glycocalyx as well as by using the biotin–(strept)avidin binding motif.[24−28]

While an increasing number of reports has explored surface modified cells as delivery systems, only relatively little effort has been made to systematically investigate and understand the effects of cell surface immobilization chemistry, particle size, and surface concentration on the properties and performance of the cell-based drug delivery systems. This study uses the noncovalent, biotin–NeutrAvidin mediated conjugation strategy[29−31] to functionalize two different T lymphocyte cell lines with fluorescent polystyrene nano- and microparticles of different sizes. From the broad variety of possible approaches, the biotin–NeutrAvidin strategy was selected as an exemplary nanoparticle–cell surface conjugation chemistry. This approach has been successfully employed in proof-of-concept studies, both in vitro and in vivo. In one example, the use of human-derived mesenchymal stem cells modified with NeutrAvidin-coated nanoparticles for the targeted delivery to tumor spheroids was demonstrated.[29] In other work, tumor-tropic neural stem cells carrying streptavidin-coated nanoparticles were shown to allow nanoparticle transport to

**Received:** January 18, 2021
**Revised:** February 11, 2021
**Published:** February 23, 2021

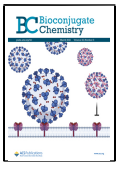







https://dx.doi.org/10.1021/acs.bioconjchem.1c00026
*Bioconjugate Chem.* 2021, 32, 541–552

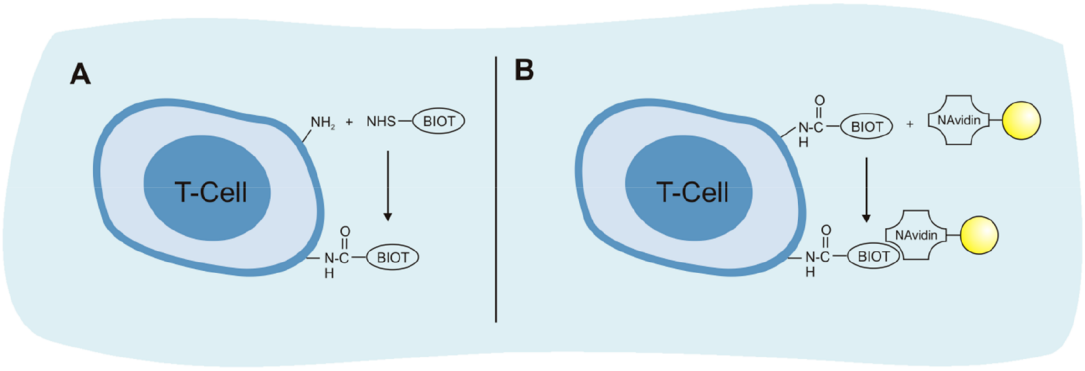


**Figure 1.** Biotin–NeutrAvidin mediated T cell surface immobilization of fluorescently labeled polystyrene nano- and microparticles. (A) T cell biotinylation using Biotin XX, SSE. (B) Attachment of NeutrAvidin (NAvidin)-coated particles on biotinylated cells.

invasive brain tumors in a mice model.[31] However, in spite of the successful use of the biotin–NeutrAvidin strategy in these proof-of-principle experiments, concerns about the immunogenicity of streptavidin may require the selection of alternative approaches for clinical use.[32] The cells used in this study, T lymphocytes, are attractive carriers for the transport of nano- and microparticulate cargo as they can possess tumor targeting and killing properties and also can serve to mediate transport across highly protective endothelial barriers, such as the blood–brain barrier (BBB). To characterize the particle decorated cells, a semiquantitative confocal microscopy method was used to analyze confocal 3D reconstructions of the cells. Using this method, the influence of particle size on the position and distribution of the particles over a period of 24 h and across the two different T cell lines was investigated. The first T cell line used was Jurkat cells, which are T lymphocytes established from an acute leukemia human patient. The Jurkat cell line is a robust cell line, which is very useful as a model system to investigate and explore various cell-surface modification strategies. The second type of T cells used was SJL/PLP7 T cells, which are primary mouse $CD4^+$ effector/memory proteolipid protein (PLP) specific ($CD4^+$ $T_{EM}$) cells. These T cells are potentially attractive as carriers to facilitate drug delivery to the central nervous system (CNS).[33] The ability of the nanoparticle decorated $CD4^+$ $T_{EM}$ cells to bind to a key protein involved in the migration across the BBB was investigated. In a second experiment, the migration of the surface-modified cells across a primary mouse brain microvascular endothelial cell (pMBMECs)-based in vitro model BBB was studied in a two chamber-based assay.[34,35]

## RESULTS AND DISCUSSION

**T Cell Surface Modification.** Figure 1 illustrates the noncovalent attachment of NeutrAvidin-coated fluorescent polystyrene nano- and microparticles on the surface of Jurkat and SJL/PLP7 T cells. For this study, NeutrAvidin-coated particles with diameters of 40 nm, 200 nm, and 1 $\mu$m were used. In a first step, biotin moieties are introduced on the T cell surface using an amine reactive biotinylating agent (Biotin-XX, SSE). After that, freshly biotinylated T cells are exposed to a NeutrAvidin-coated particle suspension for 30 min, after which the remaining free biotin binding sites are blocked with biotin-functionalized PEG and unbound particles removed by centrifugation.

Biotinylation of the T cells was typically performed by incubation of 25 mio cells/mL in DPBS and addition of Biotin-XX, SSE to a final concentration of 0.5 mM for 30 min. This procedure ensures a high biotin cell surface concentration. These optimized conditions were identified in screening experiments in which Jurkat cells were exposed to 0.05 mM, 0.5 mM, and 1.0 mM Biotin-XX, SEE. Throughout these experiments, the cell concentration and nanoparticle-to-cell ratio were kept constant at 0.5 mio cells/well and 2000 nanoparticles/cell, respectively. To validate the presence of biotin moieties on the cell surface and to monitor changes in the surface concentration of these groups upon varying the concentration of Biotin-XX, SSE, cells were treated with NeutrAvidin-Oregon Green 488 and analyzed by flow cytometry. As shown in Figure 2A, a gradual shift in the

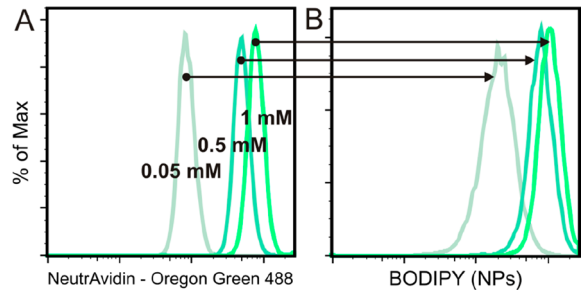


**Figure 2.** (A) Flow cytometry histograms of scatter gated live Jurkat cells stained with NeutrAvidin–Oregon Green 488 conjugate previously treated with different concentrations of biotinylating agent (Biotin-XX, SSE). (B) Flow cytometry histograms of scatter gated, biotinylated live Jurkat cells modified with 200-nm-diameter particles. The different histograms represent nanoparticle decorated cells that were obtained from cells modified with different concentrations of Biotin-XX, SSE.

NeutrAvidin-Oregon Green 488 associated fluorescence is observed when the concentration of Biotin-XX, SSE is increased from 0.05 to 1.0 mM, which is consistent with an increasing concentration of biotin groups on the cell surface. When Jurkat cells at a concentration of 0.5 mio cells/well were treated with 0.05 mM, 0.5 mM, and 1 mM Biotin-XX, SSE and subsequently exposed to a 2000-fold excess of 200 nm NeutrAvidin-coated polystyrene nanoparticles (i.e., 2000 nanoparticles/cell), a similar shift is observed in the nanoparticle-associated BODIPY fluorescence, demonstrating that the increased biotin cell surface concentration enhances the polystyrene nanoparticle binding capacity of the T cell (Figure 2B). For further experiments (*vide infra*), a concentration of 0.5 mM Biotin-XX, SSE was used. This concentration ensures sufficiently high biotinylation for subsequent nanoparticle


https://dx.doi.org/10.1021/acs.bioconjchem.1c00026
Bioconjugate Chem. 2021, 32, 541–552

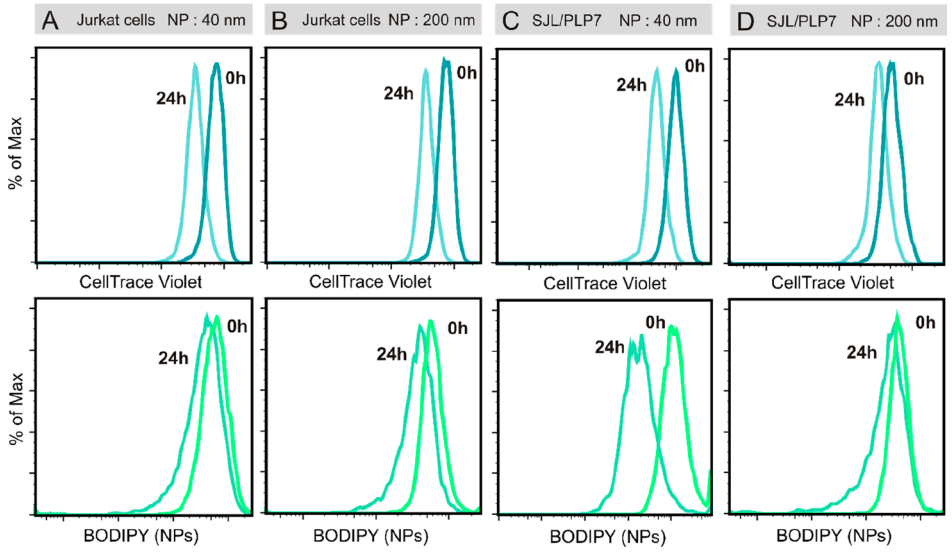


**Figure 3.** Flow cytometry histograms of scatter gated live cells directly after modification and 24 h later. Top: cell proliferation as observed using CellTrace Violet staining. Bottom: nanoparticle retention was assessed using BODIPY labeled fluorescent nanoparticles. Data are shown for Jurkat cells functionalized with 40 nm (A) and 200 nm nanoparticles (B), as well as SJL/PLP7 T cells functionalized with 40 nm (C) and 200 nm nanoparticles (D).

attachment without compromising the cell viability during this first step. The same protocol was also used for the biotinylation of the SJL/PLP7 T cells. At a concentration of 0.5 mM Biotin-XX, SSE the extent of biotinylation of these cells was approximately 1.6-fold higher than for Jurkat cells (Supporting Information Figure S1A). Cell surface biotinylation of the Jurkat and SJL/PLP7 T cells was also analyzed by confocal microscopy using Oregon Green 488 labeled NeutrAvidin to detect biotin moieties. The images show high and homogeneous NeutrAvidin-Oregon Green 488 fluorescence on the surface of Jurkat cells and SJL/PLP7 T cells (Supporting Information Figure S1B).

The cell-surface attachment protocols were subsequently adapted to 40-nm- and 1-$\mu$m-diameter NeutrAvidin-coated particles. For these experiments, cells were used that had been treated with 0.5 mM Biotin-XX, SSE. As a control, to evaluate nonspecific binding of the NeutrAvidin-coated particles, cells were used that had not been modified with Biotin-XX, SSE. For Jurkat cells, cell surface immobilization was performed using 1 mio cells/well and 200,000 nanoparticles/cell (40-nm-diameter particles) and 1 mio cells/well and 1800 particles/cell (1-$\mu$m-diameter particles). SJL/PLP7 T cells were modified at a concentration of 0.5 mio cells/well and 8000 nanoparticles/cell (200 nm particles), respectively, 1 mio cells/well and 200,000 nanoparticles/cell (40 nm particles). These concentrations of cells per well and the ratio of particles to cell were chosen such as to maximize specific, biotin−NeutrAvidin mediated binding versus nonspecific binding. Modification of the cell surfaces with the NeutrAvidin-coated particles was monitored with flow cytometry. To remove loosely bound and excess particles, cells were subjected to three centrifugal washing cycles. While this procedure was very efficient for the 40 and 200 nm particles, purification of T cells decorated with 1 $\mu$m polystyrene particles was challenging, and it was difficult to produce T cells that were free of unbound material. As a consequence, T cells modified with 1 $\mu$m particles were only characterized by confocal microscopy. To assess unspecific binding, Supporting Information Figure S2 compares flow cytometry histograms of biotinylated and nonbiotinylated T cells that were exposed to 40- and 200-nm-diameter NeutrAvidin-coated particles. Although unspecific binding takes place in all cases, a 14-fold increase in mean fluorescence intensity (MFI) was observed for 200 nm nanoparticles on biotinylated Jurkat cells versus unmodified control cells (Supporting Information Figure S2B), and a 2.7-fold increase was observed when 40 nm particles were used (Supporting Information Figure S2A). For biotinylated SJL/PLP7 T cells, an 8-fold increase in MFI was observed for 200 nm particles versus unmodified control cells (Supporting Information Figure S2C). These increases account for the specific biotin−NeutrAvidin mediated binding of nanoparticles. Since NeutrAvidin itself does not bind to nonbiotinylated T cells as observed in flow cytometry experiments (Supporting Information Figure S1A), the nonspecific binding that is observed in Supporting Information Figure S2 is attributed to interactions between the polystyrene core of the nanoparticles and the cell membrane. As mentioned before, since it was difficult to produce T cells modified with 1 $\mu$m particles that were free of unbound material, Supporting Information Figure S2 does not include data for cells modified with these particles.

Next, proliferation of the particle-modified cells was studied. To this end, cells were stained with a proliferation marker, CellTrace Violet, prior to biotinylation. CellTrace Violet is a cell-penetrating and succinimidyl ester functionalized phenolic dye. The low concentration of CellTrace Violet (5 $\mu$M for a typical staining protocol) was not found to affect the subsequent biotinylation of T cells, which was performed using a 100-fold higher concentration of the amine reactive biotinylating agent. As the nanoparticles are also fluorescently labeled, flow cytometry allows simultaneous monitoring of changes in both the CellTrace Violet as well as the nanoparticle-associated fluorescence. Figure 3 presents the results of flow cytometry measurements directly after surface modification (0 h) and 24 h later. For the nanoparticle-decorated Jurkat cells, over this time period, a 2-fold decrease in the Cell-Trace Violet associated mean fluorescence intensity was observed, suggesting that the cells go through one division cycle in 24 h. Over the same time period, for both 40 and 200


https://dx.doi.org/10.1021/acs.bioconjchem.1c00026
Bioconjugate Chem. 2021, 32, 541−552

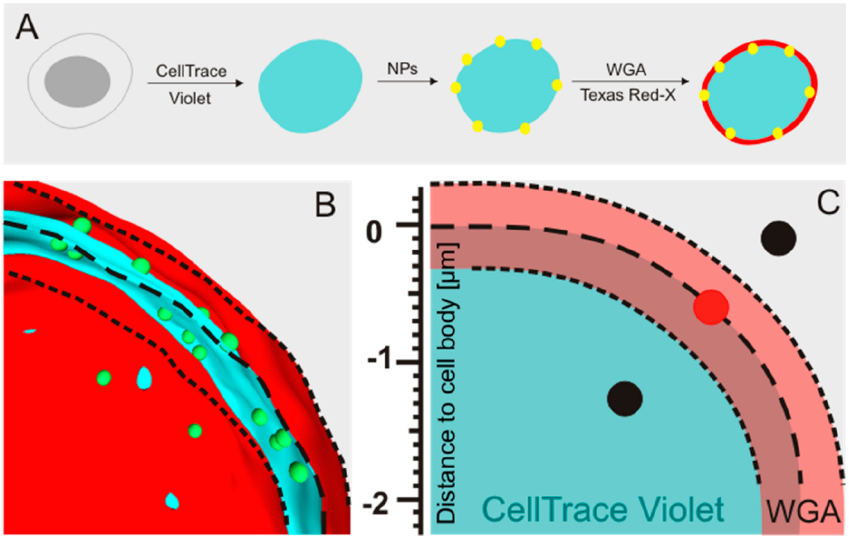


**Figure 4.** (A) Workflow for the preparation of nanoparticle (yellow) decorated T cells with a whole cell staining (cyan, CellTrace Violet) and membrane staining (red, WGA Texas Red-X). (B) Surface generated from image processing (Imaris) showing the edge of CellTrace Violet (cyan) whole cell staining (– – – – –), inner and outer bounds of the WGA-Texas Red-X (red) membrane staining (- - - - -) and 200 nm nanoparticles (green). (C) Schematic illustration of the nanoparticle distribution presented in Figure 6 around the cell edge based on 3D-reconstruction and image processing as shown in (B) (see also ref 33). The edge of CellTrace Violet (cyan) whole cell staining is represented by (– – – – –), and inner and outer bounds of the WGA-Texas Red-X (red) membrane staining as (- - - - -). When a nanoparticle appears as a red dot, this nanoparticle is colocalized with the membrane dye; otherwise, it is shown as a black dot in Figure 6.

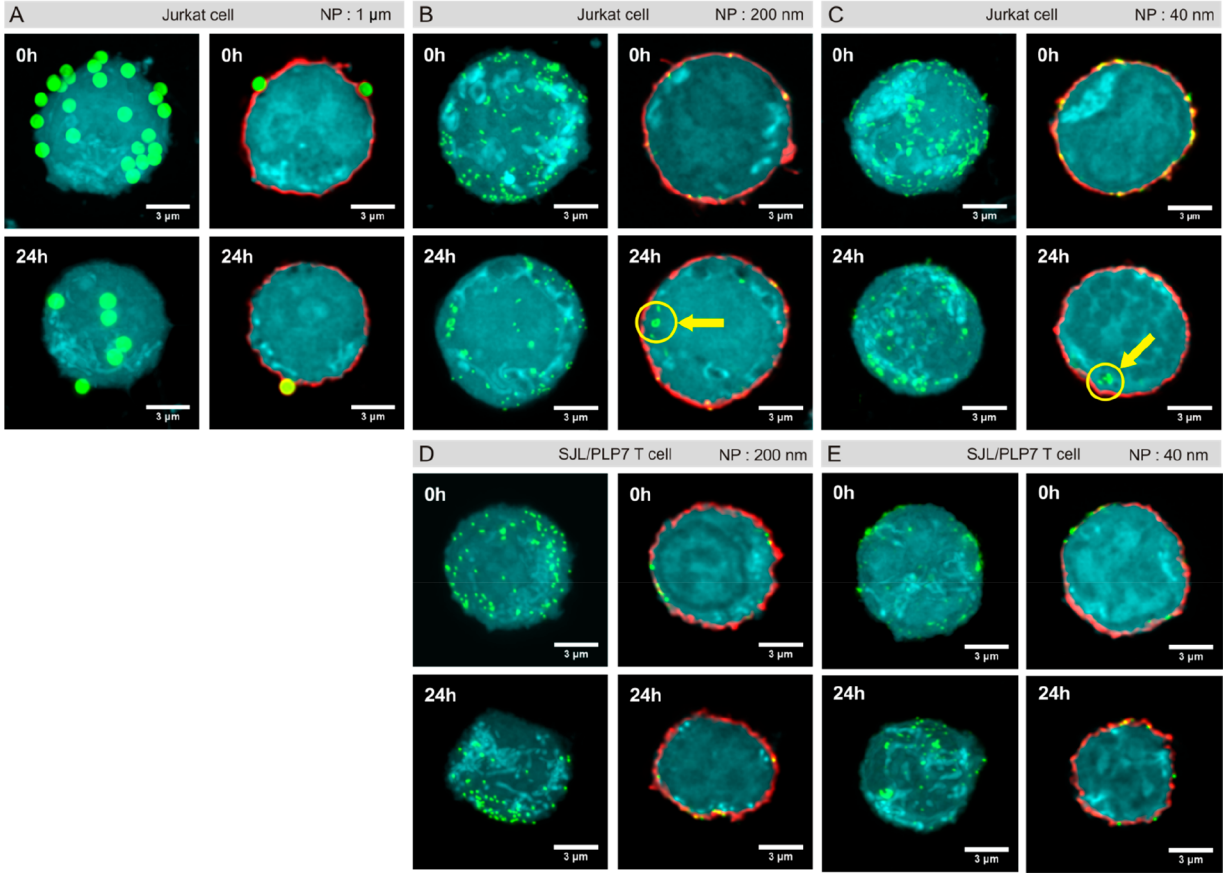


**Figure 5.** 3D-reconstructions (images on the left) of confocal micrography z-stacks of nanoparticle (green) decorated cells (cyan, CellTrace Violet) directly after modification (top) and 24 h later (bottom), as well as two 2D-images of a cross-sectional confocal plane (images on the right) of a nanoparticle modified T cell directly after modification (top) and 24 h later (bottom) showing an additional membrane WGA-Texas Red-X (red) staining. Yellow arrows indicate internalized nanoparticles. (A) Jurkat cell modified with 1 $\mu$m particles. (B) Jurkat cell modified with 200 nm particles. (C) Jurkat cell modified with 40 nm particles. (D) SJL/PLP7 T cell modified with 200 nm particles and (E) SJL/PLP7 cell modified with 40 nm particles.


https://dx.doi.org/10.1021/acs.bioconjchem.1c00026
Bioconjugate Chem. 2021, 32, 541−552

**Table 1. Particle Cell Surface Concentrations and Localization Obtained from Image Processing and Statistical Analysis of 3D Reconstructions Obtained by Confocal Microscopy (9 Cells per Condition Were Evaluated)**

| Cell line | NP size | Time (h) | NPs/cell (or PSF detections) | % NP localization between inner/outer WGA-Texas Red-X boundaries | Statistical significance[a] |
|---|---|---|---|---|---|
| Jurkat cells | 40 nm | 0 | (275 ± 84) | 92 ± 4 | *** |
| | | 24 | (142 ± 43) | 65 ± 7 | |
| | 200 nm | 0 | 124 ± 45 | 92 ± 3 | ** |
| | | 24 | 60 ± 25 | 75 ± 15 | |
| | 1 $\mu$m | 0 | 9 ± 4 | >98% | N/A |
| | | 24 | 5 ± 1 | 100 | |
| SJL/PLP7 | 40 nm | 0 | (141 ± 48) | 81 ± 9 | ns |
| | | 24 | (71 ± 66) | 77 ± 15 | |
| | 200 nm | 0 | 79 ± 19 | 87 ± 9 | * |
| | | 24 | 48 ± 14 | 96.5 ± 4.5 | |

[a]Statistical significance between percentage of nanoparticles (NPs) found within WGA-Texas Red-X boundaries directly after modification or 24 h later. *P*-values were determined by *t* test. *P*-value: (ns: $P > 0.05$; *$P \leq 0.05$; **$P \leq 0.01$; ***$P \leq 0.001$). N/A = not available.

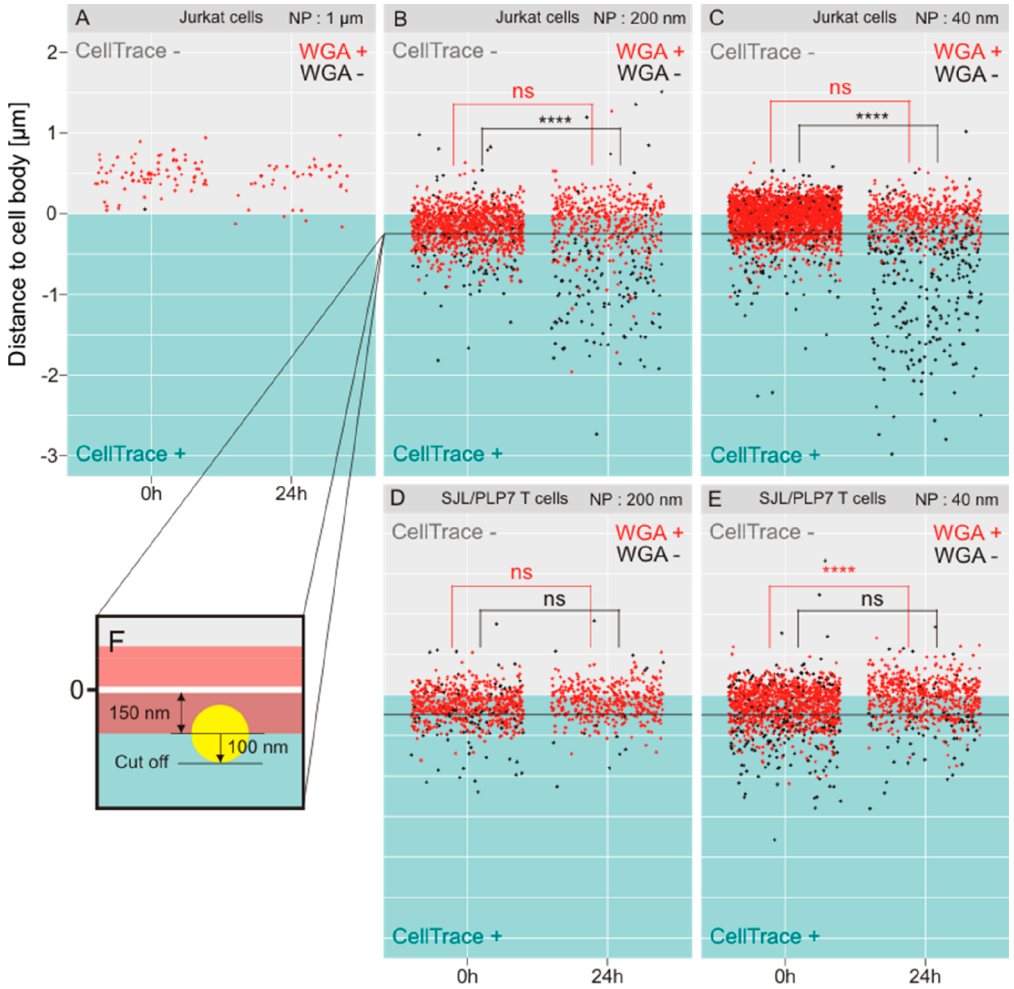


**Figure 6.** Distribution of particles with respect to their distance from the whole cell edge (CellTrace Violet). Each dot represents a single nanoparticle. Red dots represent nanoparticles, which are located between the inner and outer boundaries of the membrane staining (WGA-Texas Red-X) (see Figure 4 for details); black dots those which are not. (A) Jurkat cells decorated with 1 $\mu$m particles. (B) Jurkat cells decorated with 200 nm particles. (C) Jurkat cells decorated with 40 nm particles. (D) SJL/PLP7 T cells decorated with 200 nm particles. (E) SJL/PLP7 T cells decorated with 40 nm particles. The statistical significance was evaluated by a $\chi^2$ test (ns: $P > 0.05$; **** $P < 0.0001$) on WGA+ (red) and WGA- (black) nanoparticle subsets for the distribution below and above the cutoff threshold (solid black line) at $t = 0$ and $t = 24$ h. (F) Cutoff threshold for the distance of a particle to the membrane was set to 250 nm. It is set to half of the sum of the PSF width of the membrane WGA staining (fwhm = 300 nm) and the PSF width of a 200 or 40 nm nanoparticle (fwhm = 200 nm) with fwhm being the full width at half-maximum in the image for the respective structure.

nm particles, an approx 1.7-fold decrease in the nanoparticle (Bodipy) associated mean fluorescence intensity was observed. This decrease in nanoparticle-associated fluorescence is consistent with the redistribution of the nanoparticles over


https://dx.doi.org/10.1021/acs.bioconjchem.1c00026
Bioconjugate Chem. 2021, 32, 541−552

daughter cells after one cycle of cell division. For SJL/PLP7 T cells modified with 200 nm nanoparticles, a 2-fold decrease in the CellTrace Violet associated mean fluorescence intensity was observed, whereas SJP/PLP 7 cells decorated with 40 nm particles showed a 1.5-fold decrease over a period of 24 h. Over the same period, the nanoparticle associated mean fluorescence intensities for these cells were reduced 6.1-fold (for 40 nm particles) and 1.9-fold (for 200 nm particles).

**Characterization of the Particle-Decorated Cells.** The number of nanoparticles per cell and their position on the cell surface were determined by confocal microscopy and subsequent image processing and analysis using Imaris.[33] Figure 4A illustrates the workflow for the preparation of the T cells for the confocal microscopy experiments. In a first step, T cells were stained with CellTrace Violet. As mentioned already, CellTrace Violet is a cell-penetrating and amine-reactive dye that binds covalently to amine groups both intracellularly and on the surface of the cell and therefore delineates the entire cell structure. The use of an amine-reactive dye is particularly interesting for long-term analysis, as the dye is efficiently retained by the cell due to its covalent attachment to proteins. This first staining step was followed by biotin−NeutrAvidin mediated modification of the cell surface with the nanoparticle of interest. Finally, the surface modified cells were labeled with Wheat Germ Agglutinin-Texas Red-X (WGA-Texas Red-X). WGA is a carbohydrate binding protein that selectively recognizes sialic acid and *N*-acetylglucosaminyl residues present on the cell membrane and as such was used to mark the surface of the cell. Figure 5 shows images of Jurkat cells modified with 40 nm, 200 nm, and 1 $\mu$m particles as well as of SJL/PLP7 T cells modified with 200- and 40-nm-diameter particles. For each set, the left images show 3D reconstructions of nanoparticle decorated T cells, and the right images present a 2D cross-sectional plane through these cells. Images were recorded both directly after cell surface modification as well as 24 h later. The 2D cross-sectional images of the 1 $\mu$m particle modified Jurkat cells, which are shown in Figure 5A, indicate that these particles are located at the edge of the cell both directly after immobilization and 24 h later. While directly after surface immobilization, 40 and 200 nm particles are located almost exclusively on the edge of the Jurkat cells, the 2D cross-sectional images taken at 24 h reveal both surface-conjugated and internalized nanoparticles (yellow arrows in Figure 5B and C). Interestingly, and in contrast to the observations on the Jurkat cells, attachment of 200 or 40 nm nanoparticles on the SJL/PLP7 T cells almost only resulted in surface-bound nanoparticles. Even after 24 h, accumulation of nanoparticles inside the cell could not be observed (Figure 5D and E).

To estimate the average number of particles per cell as well as the location of the particles on the cell surface, 9 cells per condition were analyzed, both directly after cell surface modification and 24 h later using the image processing protocol outlined in Figure 4B and C. Figure 4B shows the results of a processed image to detect spheres and surfaces generated by the staining protocols. This figure shows the surface generated from the edge of CellTrace Violet staining (cyan) and both the inner and outer boundaries of the WGA staining (red) and 200 nm nanoparticles detected as spheres (green). The processed images were evaluated as illustrated in Figure 4C.[33] In brief, each particle was assigned a distance from the surface generated by the CellTrace Violet staining. The edge of the CellTrace violet is defined as 0 $\mu$m in Figure 4B and C. Positive values are attributed to nanoparticles detected outside the staining, and negative values are attributed to nanoparticles found inside the CellTrace Violet staining. The results of the image analyses are summarized in Table 1 and Figure 6. Figure 6 shows the distribution of nanoparticles with respect to their distance from the whole cell edge (CellTrace Violet). In Figure 6, nanoparticles that are detected between the inner and outer boundaries of the WGA membrane stain appear as red dots, while those that are not are shown as black. Table 1 summarizes the average number of nanoparticles per cell as well as the percentage of particles that are found in between the inner and outer boundaries of the WGA-Texas Red-X membrane stain directly after cell surface modification and after 24 h. Figure 6A shows the results for 1 $\mu$m particles on Jurkat cells. On average, directly after modification 9 ± 4 particles can be found on the surface of the cell, and 24 h later, there are 5 ± 1 particles. The particles are localized on average at a distance of 537 ± 519 nm directly after modification and at 400 ± 240 nm 24 h later, corresponding approximately to a distance equivalent to the radius of the fluorescent particles. Figure 6B illustrates the distribution of 200 nm nanoparticles on Jurkat cells. On average, there are 124 ± 45 nanoparticles per cell at $t$ = 0 and 60 ± 25 nanoparticles 24 h later. Of the 124 nanoparticles that are found on the cell surface directly after modification, 92 ± 3.2% are found within the WGA membrane dye boundaries. At $t$ = 24 h, the percentage of nanoparticles found within the WGA membrane dye boundaries decreases to 74.7 ± 14.7%, indicating that some nanoparticle internalization occurred, as can be observed from the increasing number of black dots distant from the edge of the whole cell staining (Figure 6B). Figure 6C summarizes the data obtained by analyzing 9 Jurkat cells modified with 40 nm particles. As the size of these particles is below the confocal microscopy resolution, it is important to note here that the detected ellipsoids are defined by the fwhm of the point spread function for that channel, e.g., a diameter of 200 nm in the $xy$ plane and 300 nm in the $z$ direction. Therefore, each single detected spot may in reality account for more than one nanoparticle. On average, 275 ± 84 ellipsoids at $t$ = 0 and 142 ± 43 24 h later were detected. Analysis of the distribution of the spots revealed that on average 92 ± 3.6% are localized within the WGA membrane dye boundaries directly after cell surface modification, while after 24 h, 65.2 ± 7.2% of the spots were found within the inner and outer boundaries of the membrane stain. These values indicate an even more pronounced internalization of 40 nm particles as compared to 200 nm particles on Jurkat cells. SJL/PLP7 T cells modified with 40 and 200 nm particles were analyzed using the same procedure (Figure 6D and E). On average, surface modification led to the attachment of 79 ± 19 200-nm-diameter nanoparticles per cell at $t$ = 0. On average, 87 ± 9% of the nanoparticles were found within the WGA membrane dye boundaries. After 24 h, the SJL/PLP7 T cells still carried 48 ± 14 particles/cell. At this time, 96.5 ± 4.5% of the particles are located within the WGA membrane dye boundaries. When the SJL/PLP7 cells were modified with 40 nm nanoparticles, 141 ± 48 ellipsoids/cell were found directly after modification and 71 ± 66 per cell 24 h later. Directly after cell surface modification, 81 ± 9% of the detected ellipsoids were found to be located within the WGA membrane dye boundaries. After 24 h, 77 ± 15% of ellipsoids were still found within the inner and outer boundaries of the membrane stain, which is not significantly different from the results obtained at 0 h. This contrasts with what was observed in the case of Jurkat


https://dx.doi.org/10.1021/acs.bioconjchem.1c00026
Bioconjugate Chem. 2021, 32, 541−552

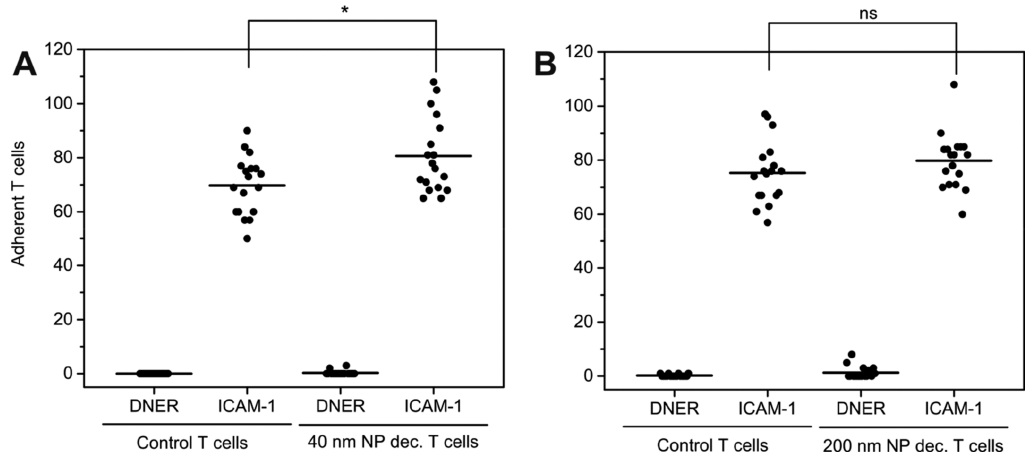


**Figure 7.** Cell count of a binding assay on ICAM-1 coated wells and DNER coated wells for unmodified control SJL/PLP7 T cells and nanoparticle (NP) decorated SJL/PLP7 T cells. (A) T cells decorated with 40 nm nanoparticles and (B) with 200 nm nanoparticles. Each dot represents one cell count from the diagonal of a 10 mm × 10 mm/10 divisions counting reticle using a 20× objective. *P*-value was determined by *t* test (ns: $P > 0.05$; * $P \leq 0.05$).

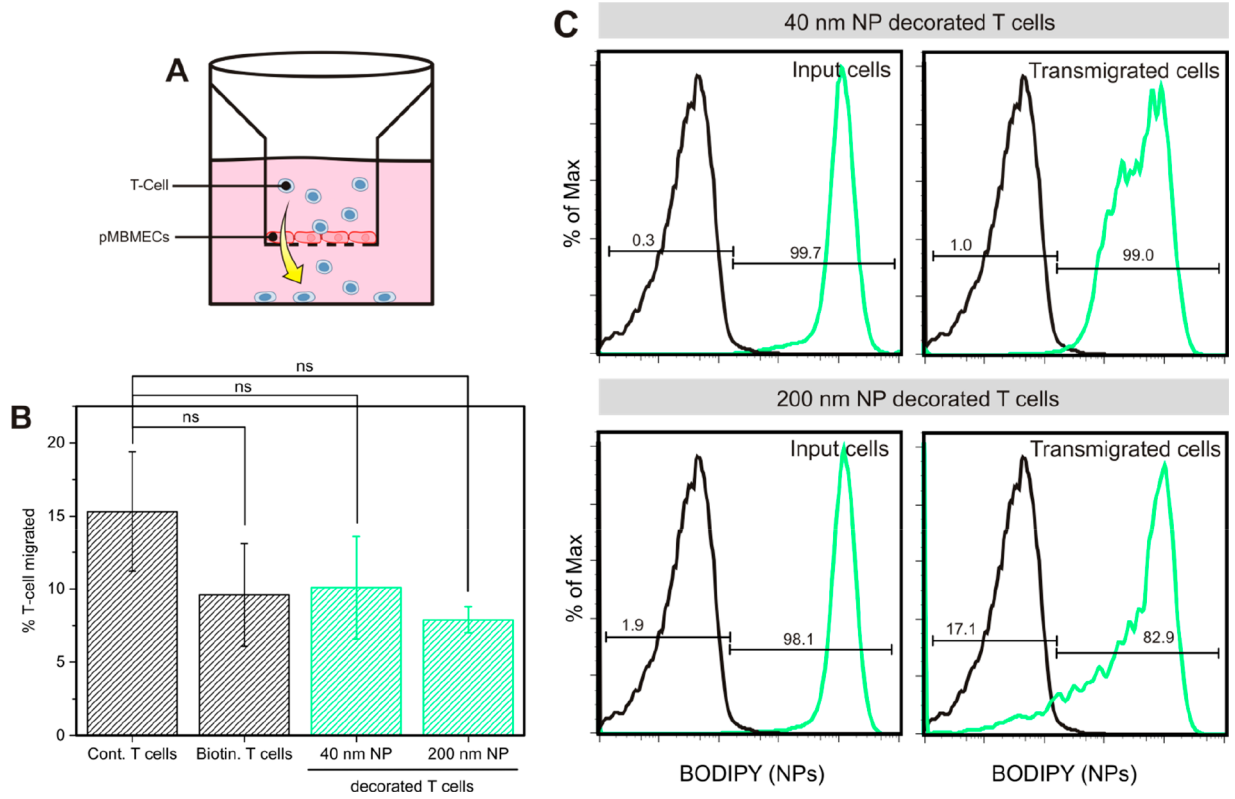


**Figure 8.** (A) Schematic overview of the two-chamber *in vitro* transendothelial migration (TEM) assay. (B) Percentage of SJL/PLP7 T cells migrated across TNF-$\alpha$ stimulated pMBMEC monolayers: comparison between unmodified control (Cont.) T cells, biotinylated (Biotin.) T cells, as well as 40- and 200-nm-nanoparticle decorated T cells. *P*-values were determined by *t* test (ns: $P > 0.05$). The histogram presents the results of one experiment performed in triplicate, and the error bars are standard deviations. (C) Flow cytometry histograms presenting the nanoparticle associated fluorescence of live scatter gated T cells: (left) T cell input for TEM assay across a TNF-$\alpha$ stimulated pMBMEC monolayer and (right) transmigrated T cells. Black: control unmodified T cells; green: 40 nm (top) and 200 nm (bottom) nanoparticle decorated T cells.

cells. The internalization of 200 and 40 nm nanoparticles was statistically analyzed with a $\chi^2$ test. To this end, a cutoff threshold was defined, as shown in Figure 6F, which was set at −250 nm considering the lowest possible point spread function (PSF) detection of a 200 or 40 nm nanoparticle (fwhm = 200 nm) localized exactly at the inner boundary of the WGA membrane stain (fwhm = 300 nm). This analysis revealed striking differences between the surface-decorated Jurkat cells on one hand and the corresponding nanoparticle decorated SJL/PLP7 cells on the other hand. In the case of the Jurkat cells, for both the 40 and 200 nm nanoparticles, a significant increase in the number of nanoparticles that were internalized by the cells was observed over a period of 24 h. For the SJL/PLP7 T cells, in contrast, the number of 40 or 200 nm particles that were located between the inner and outer WGA-Texas Red boundaries did not significantly change over 24 h. This


https://dx.doi.org/10.1021/acs.bioconjchem.1c00026
Bioconjugate Chem. 2021, 32, 541−552

reflects the differences between the Jurkat cells on one hand, which are human-derived leukemia cells, and the mouse SJL/PLP7 cells that are derived from the lymph nodes. Finally, it is worthwhile to note that in Figure 6, in almost all cases a certain number of nanoparticles detected close to the CellTrace Violet surface appear as black dots, whereas they should in principle also be localized within the boundaries of the membrane dye. This bias may happen for nanoparticles that are detected on the top or the bottom of the cells. Due to the poorer resolution in the $z$ direction, it is often the case that surfaces generated during image processing for the WGA Texas Red-X stain are discontinuous in these regions. This could in principle be avoided by exclusion of these spots during analysis.

**ICAM-1 Binding.** The SJL/PLP7 cell line is of interest since these effector/memory $CD4^+$ T lymphocytes are able to cross the BBB also in the absence of neuroinflammation.[33] This is attractive as it offers opportunities to use these T cells to facilitate delivery of nanoparticles to the CNS. One endothelial cell adhesion molecule that has been identified as crucial in the extravasation of SJL/PLP7 cells across the BBB is the intercellular adhesion molecule-1 (ICAM-1).[34,36] To investigate the ability of nanoparticle decorated SJL/PLP7 cells to recognize and bind to ICAM-1, a functional assay was performed using recombinant ICAM-1-IgG-Fc fusion protein coated diagnostic slides. As controls, nonmodified SJL/PLP7 T cells and wells modified with delta/notch-like epidermal growth factor (DNER)-IgG were used. DNER was used as a control, since this is a protein that is not relevant to the extravasation of $CD4^+$ $T_{EM}$ cells across the BBB. Figure 7 presents the number of adherent cells counted per field of view for 40 and 200 nm nanoparticle decorated SJL/PLP7 T cells and unmodified T cells on both ICAM-1 and control DNER coated surfaces. The results in Figure 7 show that biotin−NeutrAvidin mediated conjugation of 40- and 200-nm-diameter nanoparticles on the surface of SJL/PLP7 cells does not impact their ability to bind to ICAM-1. The absence of adherent T cells in the DNER coated control wells indicates that binding of the nanoparticle decorated cells is specific and thus mediated by lymphocyte function-associated antigen-1 (LFA-1) rather than driven by nonspecific interactions. No statistically significant differences in the number of cells that bind to ICAM-1 were observed when comparing 200-nm-diameter modified SJL/PLP7 cells with nonmodified cells. SJL/PLP7 cells modified with 40-nm-diameter nanoparticles were found to bind slightly more to the ICAM-1 presenting surfaces as compared to the nonmodified control cells.

**Transendothelial Migration Assay.** In a second experiment to assess the possible effect of the biotin−NeutrAvidin-mediated nanoparticle cell surface immobilization on T cell function, SJL/PLP7 cells were evaluated for their ability to cross a monolayer of primary mouse brain microvascular endothelial cells (pMBMEC) as an *in vitro* model of the BBB (Figure 8A). This established model retains BBB features *in vitro* such as complex tight junctions and low permeability.[37,38] The assay was performed on TNF-$\alpha$ stimulated pMBMEC monolayers, which increases the expression of endothelial adhesion molecules such as ICAM-1 on the surface of the pMBMECs. The assay was run for a period of 4 h. Analysis by flow cytometry showed that 15.3 ± 4.1% of control, i.e., nonmodified, SJL/PLP7 T cells migrated across the TNF-$\alpha$ stimulated pMBMEC monolayer during this period (Figure 8B). The percentages of migrated biotinylated, 40-nm-nanoparticle, and 200-nm-nanoparticle decorated T cells were 9.6 ± 3.5%, 10.1 ± 3.5%, and 7.8 ± 0.9%, respectively. Although there seems to be a slight decrease in the percentage of migrating modified T cells, these differences are not statistically different as compared to the control, nonmodified T cells. Figure 8C shows flow cytometry histograms that present the nanoparticle-associated fluorescence of SJL/PLP7 T cells modified with 40 and 200 nm nanoparticles before (input) and after transmigration. Comparison of the results of the transmigrated and input cells indicates that transmigration of nanoparticle functionalized T cells is accompanied by a 6.5-fold and 2.8-fold decrease in nanoparticle-associated fluorescence for SJL/PLP7 cells modified with 200- and 40-nm-diameter particles, respectively. This decrease in the nanoparticle-associated fluorescence indicates a partial loss of nanoparticle cargo as the T cells migrate across the pMBMEC monolayer. While in the case of the 40 nm particle payload all cells remained functionalized, ∼17% of the T cells that were modified with 200-nm-diameter particles lost their entire payload. In spite of this partial loss of nanoparticle cargo, these experiments demonstrate that biotin−NeutrAvidin mediated functionalization does not significantly impact the migratory properties of the SJL/PLP7 cells.

## ■ CONCLUSIONS

This study has investigated the effects of particle size and cell line on the biotin−NeutrAvidin mediated cell surface immobilization of model nanoparticles. For cells that were modified under identical conditions with similarly sized particles, confocal microscopy analysis revealed significantly lower nanoparticle surface concentrations for SJL/PLP7 T cells as compared to Jurkat T cells. Confocal microscopy analysis further revealed significant internalization of both 40 and 200 nm particles by Jurkat cells over a time frame of 24 h, whereas nanoparticle internalization by SJL/PLP7 cells was essentially absent. In functional assays, the ability of nanoparticle decorated cells to bind to ICAM-1 and to migrate across pMBMEC monolayers, which are key characteristics with respect to transport across the BBB, were found not to be impaired. This article demonstrates the potential of biotin−NeutrAvidin binding to noncovalently immobilize nanoparticle cargo on the surface of carrier cells that are of potential interest for delivery to the central nervous system. The results that have been presented also highlight the effects of particle size and cell line on the surface immobilization of nanoparticles on living cells.

## ■ EXPERIMENTAL SECTION

**Materials.** NeutrAvidin coated yellow−green polystyrene FluoSpheres ($d$ = 1 $\mu$m, 200 nm, and 40 nm), NeutrAvidin Oregon Green 488 conjugate, CellTrace Violet, WGA-Texas Red conjugate, 6-((6-((biotinoyl)amino)hexanoyl)amino)-hexanoic acid, sulfosuccinimidyl ester, sodium salt (Biotin-XX, SSE), Prolong Gold mounting media, Dulbecco's phosphate-buffered saline (DPBS), RPMI 1640, and FBS were purchased from Thermofischer Scientific. $mPEG_{2000}$-Biotin was obtained from Laysan Bio Inc. Poly(L-lysine) (0.1% w/v solution), paraformaldehyde (PFA), and sodium azide were purchased from Sigma-Aldrich.

**Methods.** Flow cytometry was performed on a Beckmann Coulter Gallios instrument. Confocal microscopy images were recorded on a Zeiss LSM700 Inverted microscope (Carl Zeiss, Feldbach, Switzerland). Cell-counting for binding assay was


https://dx.doi.org/10.1021/acs.bioconjchem.1c00026
Bioconjugate Chem. 2021, 32, 541−552

performed using an Olympus CKX41 inverted microscope equipped with a 10 mm × 10 mm/10 divisions counting reticle and a 20× objective.

**Procedures.** *Cell Lines and Cell Cultures. Jurkat cells* were cultured in RPMI 1640 glutamax medium (Gibco) supplemented with 10% fetal bovine serum (FBS) (Gibco), 1% penicillin/streptomycin (Gibco), 1% Na-pyruvate (Gibco). Cells were maintained between $1 \times 10^5$ and $1 \times 10^6$ cells/mL in Corning T175 flasks.

*Encephalitogenic $CD4^+$ effector/memory proteolipid protein (PLP) peptide aa139−153 specific T cells (line SJL/PLP7)* were cultured as previously described.[39] In brief, PLP-specific T cells were cultured in RPMI 1640 glutamax medium (Gibco) supplemented with 10% fetal bovine serum (FBS) (Gibco), 1% penicillin/streptomycin (Gibco), 1% nonessential amino acid (Gibco), 1% Na-pyruvate (Gibco), 0.4% $\beta$-mercaptoethanol (Gibco), and 1% IL-2 supernatant (self-made). Cells were typically used for modification and in functional assays at day 3 or 4 following a prior 3-day antigen-specific re-stimulation.

*Primary mouse brain microvascular endothelial cells (pMBMECs)* were isolated and cultured as described before.[37,38,40] In brief, cortexes from 6−8-week-old C57BL/6 mice were isolated by removing cerebellum, striatum, optic nerves, and the brain white matter. The meninges were removed using dry cotton swabs. Preparations were pooled and ground using a Dounce homogenizer with a large clearance pestle of 0.06−0.08 mm in wash buffer (HBSS containing 10 mM HEPES and 0.1% BSA). The resulting homogenate was mixed with 30% dextran (v/v, molecular weight 100,000−200,000 Da) in wash buffer. This suspension was centrifuged at 3000*g* for 25 min at 10 °C. The neural component and the dextran layer were discarded, and the pellets containing the blood vessels were filtered through a nylon mesh with 60 $\mu$m pore size. The capillary-enriched filtrate was digested in collagenase/Dispase (2 mg/mL) in wash buffer supplemented with 10 $\mu$g/mL DNase I and 0.147 $\mu$g/mL TLCK (tosyl-L-lysyl-chloromethane hydrochloride) for 30 min at 37 °C. Digestion was stopped by adding an excess of wash buffer, and the suspension was filtered through a nylon mesh of 20 $\mu$m pore size. The resulting digested capillary suspension was seeded onto Matrigel-coated tissue culture dishes or Transwell inserts. Culture medium was DMEM supplemented with 20% FBS, 2% sodium pyruvate, 2% nonessential amino acids, 50 $\mu$g/mL gentamycin, and 1 ng/mL basic fibroblast growth factor supplemented during the first 48 h with 4 $\mu$g/mL puromycin. Twenty-four hours after plating, red blood cells, cell debris, and nonadherent cells were removed by washing with medium. Afterward, the medium was changed every second day and pMBMECs were used on day 7 or 8 after isolation.

*Biotinylation of T Cells.* First, T cells were washed 3× with DPBS (centrifuged at 250*g* for 7 min) and finally resuspended at a concentration of 25 mio cells/mL in DPBS. Cells were left to cool on ice for at least 5 min before Biotin-XX, SSE, a cell-impermeable *N*-sulfosuccinimidyl reactive ester (Thermofisher scientific) was added to the cell suspension to a final concentration of approximately 0.05 mM, 0.5 mM, or 1 mM. Cells were functionalized on ice for 30 min and then washed three times with DPBS and used directly for nanoparticle conjugation. The biotinylation of T cells was monitored by flow cytometry. In short, 0.5 mio cells were resuspended in 1 mL FACS buffer (DPBS, 2.5% FBS, 0.1% sodium azide) containing 10 $\mu$L of a 1 mg/mL solution of NeutrAvidin Oregon Green 488 conjugate and left on ice for 20 min in the dark, washed once with FACS buffer, and resuspended in 1% PFA in DPBS for analysis.

*T Cell Surface Modification with NeutrAvidin Coated Fluorescent Nanoparticles.* Freshly biotinylated T cells were resuspended at a concentration of 5 or 10 mio cells/mL in DPBS. Then, 100 $\mu$L cell suspension (i.e., 0.5 to 1 mio cells) was added to each well (Greiner Bio-One, 96 well round-bottom plate, with cell-repellent surface) followed by addition of 100 $\mu$L nanoparticle suspension. Nanoparticle solutions were prepared at a defined concentration according to the conditions for each particle size and cell line listed below. The conjugation was performed at room temperature, in the absence of light for 30 min with gentle pipet mixing every 10 min. After the conjugation, the remaining binding sites were blocked by adding the cell and nanoparticle suspension to a solution of 10 mg/mL Biotin-$PEG_{2000}$-OMe and left at room temperature for another 10 min at 37 °C. Subsequently, cells were washed 3× with approximately 10 mL DPBS (centrifuged at 250*g* for 7 min) to remove unbound and loosely bound particles. Cells were then either resuspended in growth media or in 1% PFA in DPBS for flow cytometry or prepared for confocal microscopy. Specific conditions for each experiment are as follows:

For Jurkat cells, 200 nm nanoparticles: 0.5 mio cells/well with 2000 nanoparticles/cell. 40 nm nanoparticles: 1 mio cells/well with 200,000 nanoparticles/cell. For 1 $\mu$m nanoparticles: 1 mio cells/well with 1800 nanoparticles/cell.

SJL/PLP7 T cells were functionalized with 200 nm nanoparticles in the following conditions: 0.5 mio cells/well and 8000 nanoparticles/cell and 40 nm nanoparticles using 1 mio cells/well and 200,000 nanoparticles/cell.

*Proliferation Assay.* T-cell proliferation was monitored with CellTrace Violet according to the manufacturer's protocol. In short, cells were washed once and resuspended in DPBS at a concentration of 1 mio cells/mL. Then, 1 $\mu$L of CellTrace Violet stock solution in DMSO (5 mM) was added per milliliter of cell suspension and left for 20 min at 37 °C in the dark. Excess dye was removed by addition of approximately 5 times the staining volume of complete growth medium. Cells were then pelleted, washed once with DPBS, and resuspended in complete growth medium until used for cell-surface modification experiments. Fluorescence intensities were measured by flow cytometry, directly after surface modification and 24 h after modification.

*Confocal Microscopy and Image Analysis.* Surface-modified and CellTrace Violet stained T cells were additionally stained with a membrane marker, WGA-Texas Red-X for 30 min on ice in DPBS at a concentration of 1 mio cells/mL. Cells were then seeded on a poly(L-lysine) coated 12-mm-diameter, 0.17-mm-thickness borosilicate glass precision microscopy coverslip (Carl Roth GmbH), washed twice with DPBS and fixed for 10 min with a 4% paraformaldehyde solution in DPBS at room temperature. Fixed cells were finally mounted on a microscopy glass slide with Prolong Gold. The slides were left to cure overnight before images were acquired on a Zeiss LSM700 microscope with a 63×/1.4NA lens. Voxel sizes were optimized for deconvolution (XYZ 30 nm × 30 nm × 130 nm) as recommended by the SVI Nyquist Calculator (https://svi.nl/NyquistCalculator). Pinhole size was matched between channels so that the slice thickness remained constant and was set as follows for each channel: 49 $\mu$m for the whole cell channel (CellTrace Violet), 48 $\mu$m for the membrane channel


https://dx.doi.org/10.1021/acs.bioconjchem.1c00026
Bioconjugate Chem. 2021, 32, 541−552

(WGA-Texas Red-X), and 47 μm for the nanoparticle channel (BODIPY). Gain was optimized for each z-stack to compensate for staining variability and to ensure the quality of detection. Deconvolution was performed with Huygens Software (Scientific Volume Imaging) using the classic maximum likelihood estimation algorithm. Signal-to-noise ratios after 40 iterations were 10, 15, and 15 for the whole cell channel (CellTrace Violet), the membrane channel (WGA-Texas Red-X), and the nanoparticle channel (BODIPY), respectively. Quality threshold was 0.1 for all channels. Image analysis was performed in Imaris (Bitplane AG, v 7.6.5) using a custom-built XTension in Matlab. Shortly, the Imaris Surface Detection Algorithm was used to detect the surfaces corresponding to the whole cell and membrane channels. Separately, the Imaris Spot Detector was used to find the locations of the nanoparticle channels. For each of the two previously detected surfaces, a Euclidean distance map was calculated from the edge of the surface. By querying the value of the distance map at each detected nanoparticle, the distance to the cell edge or to the membrane was obtained. Whether the nanoparticles are inside or outside is represented by either positive or negative distance values, respectively.

*T Cell Binding to ICAM-1.* ICAM-1 coated slides were prepared as previously reported.[41] In brief, standard 12 well diagnostic slides (ER-202W-CE24, ThermoFisher Scientific) were coated with a protein A (BioVision, Lausen, Switzerland) solution at a concentration of 20 μg/mL in PBS (pH 9) for 1 h at 37 °C. The protein A incubation was followed by three PBS washes and subsequently a blocking step using 1.5% bovine serum albumin (BSA) in PBS overnight at 4 °C. Wells were then washed once with PBS (pH 7.4), and protein A was exposed to recombinant purified 100 nM mouse ICAM-1-IgG-Fc chimera (R&D Systems, Abingdon, U.K.) for 2 h at 37 °C, and finally the wells were blocked with 1.5% BSA in PBS for 30 min at room temperature and washed once with PBS before use in a binding assay. As a control, a DNER-IgG-Fc (R&D Systems, Abingdon, U.K.) chimera was used instead of a mouse ICAM-1-Fc chimera.

For the binding assay, SJL/PLP7 T cells were collected at 10 mio cells/mL in migration assay medium (MAM: DMEM, 25 mM HEPES, 5% FBS, 2% L-glutamine) and $1 \times 10^5$ cells were added to each well and the slide was incubated for 30 min at room temperature on a rotating platform. The slides were finally washed twice by dipping them into PBS and fixed for 2 h in 2.5% v/v glutaraldehyde in PBS. The number of adherent cells was evaluated by counting the number of bound cells per field of view using a 20× objective mounted on an Olympus CKX41 inverted microscope equipped with a 10 mm × 10 mm/10 divisions counting reticle. Each dot in Figure 7 represents a single cell count from the diagonal of the reticle; three counts per well (i.e., per replicate) were recorded in a total of two independent experiments performed in triplicate).

*Transendothelial Migration Assay under Static Conditions.* Transmigration assays were performed as described before[42] using a two-chamber Transwell system. In brief, pMBMECs were seeded on 6.5 mm Transwell filter inserts with a 5 μm pore size (Costar, Bodenheim, Germany) previously coated with laminin and cytokine-depleted Matrigel. In order to prevent the pMBMECs from sprouting through the pores of the filter, they were grown to confluency without medium in the lower compartment. Prior to the experiment, pMBMECs were stimulated with recombinant mouse tumor necrosis factor alpha, TNF-α (10 ng/mL) for 16 h. At the beginning of the transmigration assay, pMBMEC inserts were washed twice with migration assay medium (MAM: DMEM (Gibco), 2% L-glutamine, 25 mM HEPES (Gibco), 5% FBS (Gibco)) before being transferred into a new 24-well Costar plate well containing 600 μL MAM. Then, 100 μL MAM containing 100,000 T cells were added per Transwell insert and T cells were allowed to transmigrate for 4 h at 37 °C. Additionally, aliquots of 100,000 T cells were kept in 600 μL MAM and used to represent the input. The number of transmigrated T cells and the number of T cells in the input samples were assessed by flow cytometry (FACS calibur) using BD Trucount tubes (BD biosciences). The percentage of migrated T cells was calculated referring to the inputs as 100%. Finally, the insets were washed twice in PBS and fixed in 1% PFA. Fixed inserts were stained with phalloidin−rhodamine and DAPI and mounted on glass slides in order to confirm the confluency of the endothelial monolayer of each filter after the assay.

## ■ ASSOCIATED CONTENT

### Supporting Information

The Supporting Information is available free of charge at https://pubs.acs.org/doi/10.1021/acs.bioconjchem.1c00026.

Additional flow cytometry and confocal microscopy analyses (PDF)

## ■ AUTHOR INFORMATION


### Corresponding Authors

**Britta Engelhardt** − *Theodor Kocher Institute, University of Bern, CH-3012 Bern, Switzerland*; Email: bengel@tki.unibe.ch

**Harm-Anton Klok** − *École Polytechnique Fédérale de Lausanne (EPFL), Institut des Matériaux and Institut des Sciences et Ingénierie Chimiques, Laboratoire des Polymères, CH-1015 Lausanne, Switzerland*; orcid.org/0000-0003-3365-6543; Email: harm-anton.klok@epfl.ch

### Authors

**Maxime Ayer** − *École Polytechnique Fédérale de Lausanne (EPFL), Institut des Matériaux and Institut des Sciences et Ingénierie Chimiques, Laboratoire des Polymères, CH-1015 Lausanne, Switzerland*

**Olivier Burri** − *École Polytechnique Fédérale de Lausanne (EPFL), Faculté des Sciences de la Vie, Bioimaging and Optics Platform, CH-1015 Lausanne, Switzerland*

**Romain Guiet** − *École Polytechnique Fédérale de Lausanne (EPFL), Faculté des Sciences de la Vie, Bioimaging and Optics Platform, CH-1015 Lausanne, Switzerland*

**Arne Seitz** − *École Polytechnique Fédérale de Lausanne (EPFL), Faculté des Sciences de la Vie, Bioimaging and Optics Platform, CH-1015 Lausanne, Switzerland*

**Elisa Kaba** − *Theodor Kocher Institute, University of Bern, CH-3012 Bern, Switzerland*

Complete contact information is available at: https://pubs.acs.org/10.1021/acs.bioconjchem.1c00026


### Notes

The authors declare no competing financial interest.

## ■ ACKNOWLEDGMENTS

The authors gratefully acknowledge financial support from the Swiss National Science Foundation (SNSF) and the European

Union Horizon 2020 MSCA-ITN-215 675619 (BtRAIN). The Supramolecular Nanomaterials and Interfaces Laboratory (SUNMIL) at EPFL is acknowledged for providing the Jurkat cells and M. Garcia from the EPFL Flow Cytometry Core Facility (FCCF) for expert help.

## REFERENCES

(1) Stephan, M. T., and Irvine, D. J. (2011) Enhancing cell therapies from the outside in: Cell surface engineering using synthetic nanomaterials. *Nano Today 6* (3), 309−325.
(2) Yoo, J.-W., Irvine, D. J., Discher, D. E., and Mitragotri, S. (2011) Bio-inspired, bioengineered and biomimetic drug delivery carriers. *Nat. Rev. Drug Discovery 10* (7), 521−535.
(3) Anselmo, A. C., and Mitragotri, S. (2014) Cell-mediated delivery of nanoparticles: Taking advantage of circulatory cells to target nanoparticles. *J. Controlled Release 190*, 531−541.
(4) Su, Y., Xie, Z., Kim, G. B., Dong, C., and Yang, J. (2015) Design strategies and applications of circulating cell-mediated drug delivery systems. *ACS Biomater. Sci. Eng. 1* (4), 201−217.
(5) Fliervoet, L. A. L., and Mastrobattista, E. (2016) Drug delivery with living cells. *Adv. Drug Delivery Rev. 106*, 63−72.
(6) Villa, C. H., Anselmo, A. C., Mitragotri, S., and Muzykantov, V. (2016) Red blood cells: Supercarriers for drugs, biologicals, and nanoparticles and inspiration for advanced delivery systems. *Adv. Drug Delivery Rev. 106*, 88−103.
(7) Ayer, M., and Klok, H.-A. (2017) Cell-mediated delivery of synthetic nano- and microparticles. *J. Controlled Release 259*, 92−104.
(8) Singh, B., and Mitragotri, S. (2020) Harnessing cells to deliver nanoparticle drugs to treat cancer. *Biotechnol. Adv. 42*, 107339.
(9) Banskota, S., Yousefpour, P., and Chilkoti, A. (2017) Cell-Based Biohybrid Drug Delivery Systems: The Best of the Synthetic and Natural Worlds. *Macromol. Biosci. 17* (1), 1600361.
(10) Pang, L., Zhang, C., Qin, J., Han, L., Li, R., Hong, C., He, H., and Wang, J. (2017) A novel strategy to achieve effective drug delivery: exploit cells as carrier combined with nanoparticles. *Drug Delivery 24* (1), 83−91.
(11) Zhao, Z., Ukidve, A., Kim, J., and Mitragotri, S. (2020) Targeting Strategies for Tissue-Specific Drug Delivery. *Cell 181* (1), 151−167.
(12) Agrahari, V., Agrahari, V., and Mitra, A. K. (2017) Next generation drug delivery: circulatory cells-mediated nanotherapeutic approaches. *Expert Opin. Drug Delivery 14* (3), 285−289.
(13) Han, X., Wang, C., and Liu, Z. (2018) Red Blood Cells as Smart Delivery Systems. *Bioconjugate Chem. 29* (4), 852−860.
(14) Chu, D., Dong, X., Shi, X., Zhang, C., and Wang, Z. (2018) Neutrophil-Based Drug Delivery Systems. *Adv. Mater. 30*, 1706245.
(15) Combes, F., Meyer, E., and Sanders, N. N. (2020) Immune cells as tumor drug delivery vehicles. *J. Controlled Release 327*, 70−87.
(16) Huang, B., Abraham, W. D., Zheng, Y., Bustamante Lopez, S. C., Luo, S. S., and Irvine, D. J. (2015) Active targeting of chemotherapy to disseminated tumors using nanoparticle-carrying T cells. *Sci. Transl. Med. 7* (291), 291ra294.
(17) Chambers, E., and Mitragotri, S. (2004) Prolonged circulation of large polymeric nanoparticles by non-covalent adsorption on erythrocytes. *J. Controlled Release 100* (1), 111−119.
(18) Timin, A. S., Litvak, M. M., Gorin, D. A., Atochina-Vasserman, E. N., Atochin, D. N., and Sukhorukov, G. B. (2018) Cell-Based Drug Delivery and Use of Nano-and Microcarriers for Cell Functionalization. *Adv. Healthcare Mater. 7* (3), 1700818−1700837.
(19) Park, J., Andrade, B., Seo, Y., Kim, M.-J., Zimmerman, S. C., and Kong, H. (2018) Engineering the Surface of Therapeutic "Living" Cells. *Chem. Rev. 118* (4), 1664−1690.
(20) Lee, D. Y., Cha, B.-H., Jung, M., Kim, A. S., Bull, D. A., and Won, Y.-W. (2018) Cell surface engineering and application in cell delivery to heart diseases. *J. Biol. Eng. 12*, 28−28.
(21) Bi, X., Yin, J., Chen Guanbang, A., and Liu, C. F. (2018) Chemical and Enzymatic Strategies for Bacterial and Mammalian Cell Surface Engineering. *Chem. - Eur. J. 24* (32), 8042−8050.
(22) Abbina, S., Siren, E. M. J., Moon, H., and Kizhakkedathu, J. N. (2018) Surface Engineering for Cell-Based Therapies: Techniques for Manipulating Mammalian Cell Surfaces. *ACS Biomater. Sci. Eng. 4* (11), 3658−3677.
(23) Custódio, C. A., and Mano, J. F. (2016) Cell Surface Engineering to Control Cellular Interactions. *ChemNanoMat 2* (5), 376−384.
(24) Pan, D. C., Myerson, J. W., Brenner, J. S., Patel, P. N., Anselmo, A. C., Mitragotri, S., and Muzykantov, V. (2018) Nanoparticle Properties Modulate Their Attachment and Effect on Carrier Red Blood Cells. *Sci. Rep. 8* (1), 1615.
(25) Swiston, A. J., Cheng, C., Um, S. H., Irvine, D. J., Cohen, R. E., and Rubner, M. F. (2008) Surface Functionalization of Living Cells with Multilayer Patches. *Nano Lett. 8* (12), 4446−4453.
(26) Doshi, N., Swiston, A. J., Gilbert, J. B., Alcaraz, M. L., Cohen, R. E., Rubner, M. F., and Mitragotri, S. (2011) Cell-Based Drug Delivery Devices Using Phagocytosis-Resistant Backpacks. *Adv. Mater. 23* (12), H105−H109.
(27) Ahmed, K. K., Geary, S. M., and Salem, A. K. (2017) Surface engineering tumor cells with adjuvant-loaded particles for use as cancer vaccines. *J. Controlled Release 248*, 1−9.
(28) Zheng, Y., Tang, L., Mabardi, L., Kumari, S., and Irvine, D. J. (2017) Enhancing Adoptive Cell Therapy of Cancer through Targeted Delivery of Small-Molecule Immunomodulators to Internalizing or Noninternalizing Receptors. *ACS Nano 11* (3), 3089−3100.
(29) Cheng, H., Kastrup, C. J., Ramanathan, R., Siegwart, D. J., Ma, M., Bogatyrev, S. R., Xu, Q. B., Whitehead, K. A., Langer, R., and Anderson, D. G. (2010) Nanoparticulate Cellular Patches for Cell-Mediated Tumoritropic Delivery. *ACS Nano 4* (2), 625−731.
(30) Mooney, R., Weng, Y., Garcia, E., Bhojane, S., Smith-Powell, L., Kim, S. U., Annala, A. J., Aboody, K. S., and Berlin, J. M. (2014) Conjugation of pH-responsive nanoparticles to neural stem cells improves intratumoral therapy. *J. Controlled Release 191* (10), 82−89.
(31) Mooney, R., Weng, Y. M., Tirughana-Sambandan, R., Valenzuela, V., Aramburo, S., Garcia, E., Li, Z. Q., Gutova, M., Annala, A. J., Berlin, J. M., et al. (2014) Neural stem cells improve intracranial nanoparticle retention and tumor-selective distribution. *Future Oncol. 10* (3), 401−415.
(32) Meyer, D. L., Schultz, J., Lin, Y., Henry, A., Sanderson, J., Jackson, J. M., Goshorn, S., Rees, A. R., and Graves, S. S. (2001) Reduced antibody response to streptavidin through site-directed mutagenesis. *Protein Sci. 10* (3), 491−503.
(33) Ayer, M., Schuster, M., Gruber, I., Blatti, C., Kaba, E., Enzmann, G., Burri, O., Guiet, R., Seitz, A., Engelhardt, B., et al. (2021) T Cell-Mediated Transport of Polymer Nanoparticles across the Blood-Brain Barrier. *Adv. Healthcare Mater. 10* (2), 2001375.
(34) Steiner, O., Coisne, C., Cecchelli, R., Boscacci, R., Deutsch, U., Engelhardt, B., and Lyck, R. (2010) Differential Roles for Endothelial ICAM-1, ICAM-2, and VCAM-1 in Shear-Resistant T Cell Arrest, Polarization, and Directed Crawling on Blood-Brain Barrier Endothelium. *J. Immunol. 185* (8), 4846−4855.
(35) Engelhardt, B., and Ransohoff, R. M. (2005) The ins and outs of T-lymphocyte trafficking to the CNS: anatomical sites and molecular mechanisms. *Trends Immunol. 26* (9), 485−495.
(36) Reiss, Y., Hoch, G., Deutsch, U., and Engelhardt, B. (1998) T cell interaction with ICAM-1-deficient endothelium in vitro: essential role for ICAM-1 and ICAM-2 in transendothelial migration of T cells. *Eur. J. Immunol. 28* (10), 3086−3099.
(37) Steiner, O., Coisne, C., Engelhardt, B., and Lyck, R. (2011) Comparison of immortalized bEnd5 and primary mouse brain microvascular endothelial cells as in vitro blood-brain barrier models for the study of T cell extravasation. *J. Cereb. Blood Flow Metab. 31* (1), 315−327.
(38) Coisne, C., Dehouck, L., Faveeuw, C., Delplace, Y., Miller, F., Landry, C., Morissette, C., Fenart, L., Cecchelli, R., Tremblay, P., et al. (2005) Mouse syngenic in vitro blood-brain barrier model: a new tool to examine inflammatory events in cerebral endothelium. *Lab. Invest. 85* (6), 734−746.


https://dx.doi.org/10.1021/acs.bioconjchem.1c00026
*Bioconjugate Chem.* 2021, 32, 541−552

(39) Engelhardt, B., Laschinger, M., Schulz, M., Samulowitz, U., Vestweber, D., and Hoch, G. (1998) The development of experimental autoimmune encephalomyelitis in the mouse requires alpha 4-integrin but not alpha 4 beta 7-integrin. *J. Clin. Invest. 102* (12), 2096−2105.
(40) Lyck, R., Ruderisch, N., Moll, A. G., Steiner, O., Cohen, C. D., Engelhardt, B., Makrides, V., and Verrey, F. (2009) Culture-induced changes in blood-brain barrier transcriptome: implications for amino-acid transporters in vivo. *J. Cereb. Blood Flow Metab. 29* (9), 1491−1502.
(41) Martin-Blondel, G., Pignolet, B., Tietz, S., Yshii, L., Gebauer, C., Perinat, T., Van Weddingen, I., Blatti, C., Engelhardt, B., and Liblau, R. (2015) Migration of encephalitogenic CD8 T cells into the central nervous system is dependent on the alpha 4 beta 1-integrin. *Eur. J. Immunol. 45* (12), 3302−3312.
(42) Röhnelt, R. K., Hoch, G., Reiss, Y., and Engelhardt, B. (1997) Immunosurveillance modelled in vitro: naive and memory T cells spontaneously migrate across unstimulated microvascular endothelium. *Int. Immunol. 9* (3), 435−450.


https://dx.doi.org/10.1021/acs.bioconjchem.1c00026
*Bioconjugate Chem.* 2021, 32, 541−552